CHAPTER 3

RESULTS AND DISCUSSION

3.1. Molybdenum Oxide synthesized by a Hydrothermal method

3.1.1 α-MoO_3 nanobelts synthesized by hydrothermal reaction at 180 °C for 20h.

3.1.1.1 X-ray diffraction

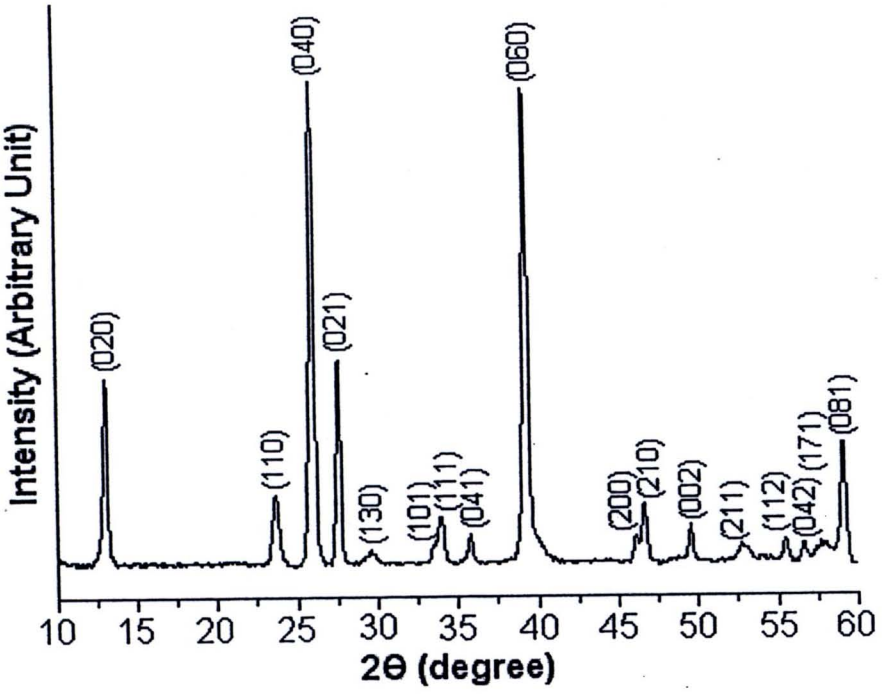

Figure 3.1 XRD pattern of α-MoO_3 nanostructure synthesized by hydrothermal reaction at 180 °C for 20 h.

The as-synthesized MoO_3 product was characterized by XRD in order to identify the phase and structure of the product. Figure 3.1 shows the XRD pattern of the MoO_3 product synthesized by hydrothermal method under 180 °C for 20 h using $(NH_4)_6Mo_7O_{24}\cdot 4H_2O$ as molybdenum source and followed by 15 ml 2 M HNO_3 adding. All the diffraction peaks of the product were identified to correspond with orthorhombic MoO_3 (α-MoO_3) of the JCPDS No. 05-0508 [30]. It is worth to note that the intensities in the family (0k0) planes with k = 2, 4, and 6 are higher than those of the standard, implying that the α-MoO_3 product is a layered crystal structure, or preferred orientation along the b axis [31].

3.1.1.2 Scanning electron microscope and transmition electron microscope

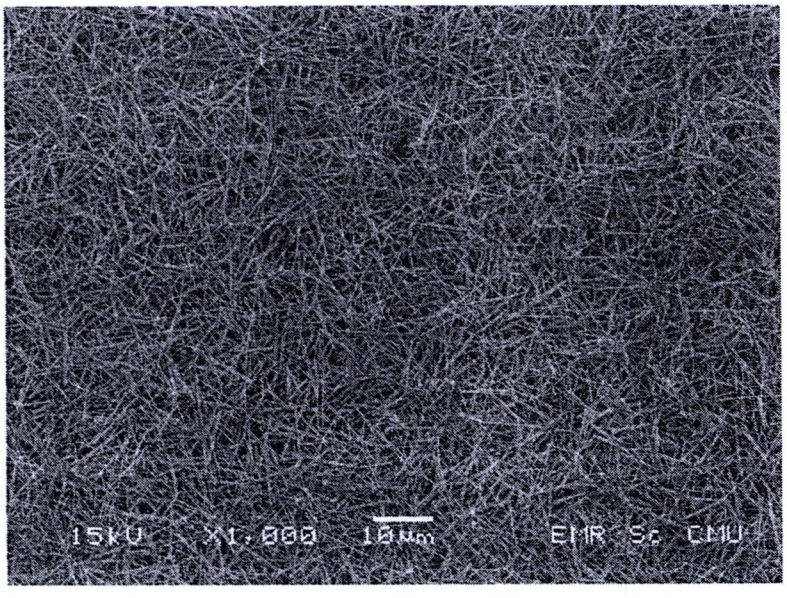

Figure 3.2 SEM image of α-MoO_3 at low magnification

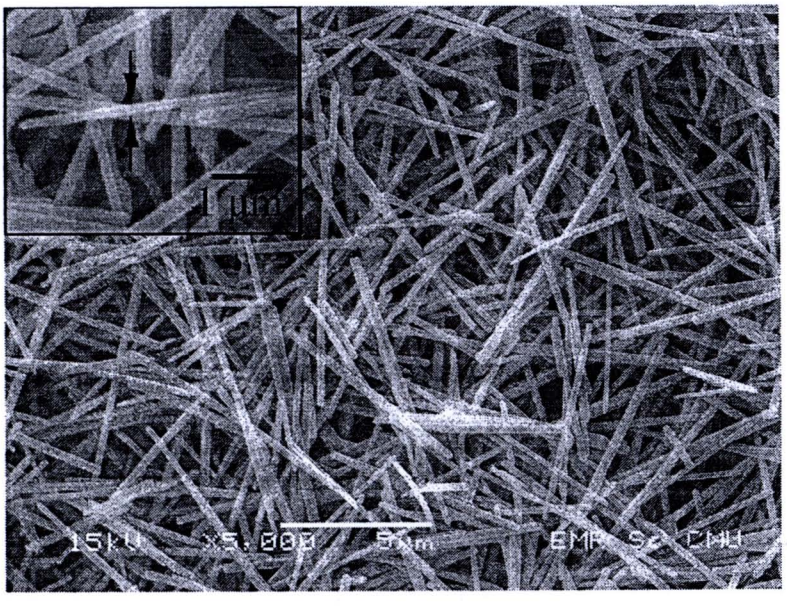

Figure 3.3 SEM image of α-MoO_3 at high magnification

Figure 3.2 and3.3 shows the high and low magnification SEM images of α-MoO_3. At low magnification, product (Figure 3.2) is completely uniform α-MoO_3 nanobelts with no detection of any other morphologies. Their lengths are more than 10 μm, and their widths are 200-250 nm. Comparison to the α-MoO_3 nanobelts hydrothermally synthesized by other researchers is summarized in Table 3.1. The present research is at an advantage in synthesizing these α-MoO_3 nanobelts without using any surfactants or templates in controlling nanobelt structure. The high magnification SEM image (Figure 3.3) shows that the surfaces of α-MoO_3 nanobelts are very smooth. A typical nanobelt is 100-120 nm thick.

Table 3.1 The α-MoO_3 nanostructures synthesized by hydrothermal reaction.

Researcher	Mo Source	Polymer	Temperature (^oC)	Time (h)	Morphology	Length (μm)	Width (nm)
S. Wang et al.[31]	$(NH_4)_6Mo_7O_{24}\cdot 4H_2O$	CTAB	180	20	Nanobelts	5	200-300
Ch.V. Subba Reddy et al.[27]	$(NH_4)_6Mo_7O_{24}\cdot 4H_2O$	PEG	180	96	Nanobelts	1-6	100-600
V.M. Mohan et al.[32]	$(NH_4)_6Mo_7O_{24}\cdot 4H_2O$	PEG	180	48	Nanobelts	0.2	70-210
Ch.V. Subba Reddy et al.[26]	$(NH_4)_6Mo_7O_{24}\cdot 4H_2O$	PVP	180	360	Nanowires	10	150
Our work	$(NH_4)_6Mo_7O_{24}\cdot 4H_2O$	Free	180	20	Nanobelts	10	200-250

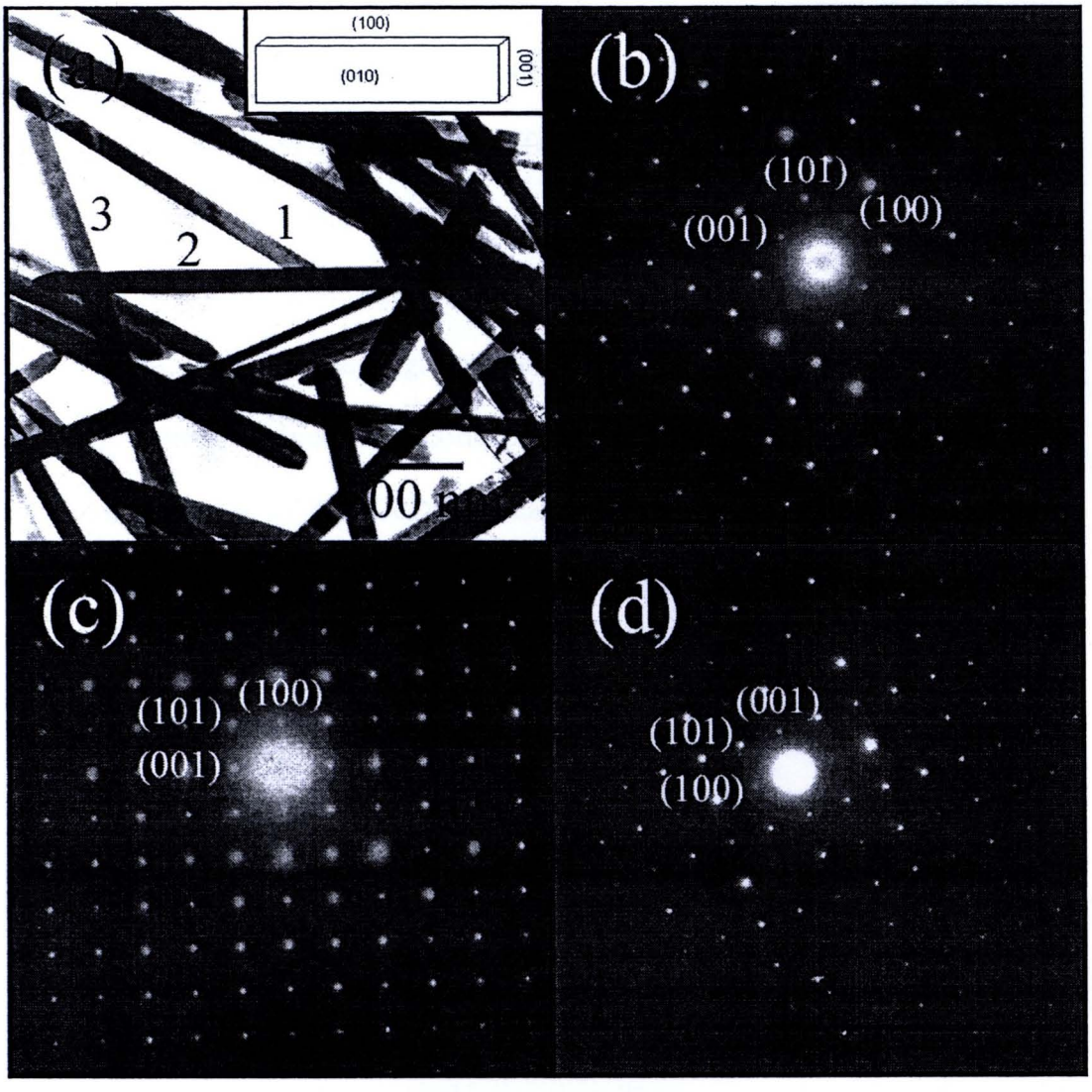

Figure 3.4 (a) TEM image and (b-d) SEAD patterns at the 1, 2 and 3 areas of α-MoO_3 nanobelts.

TEM image of α-MoO_3 (Figure 3.4a) shows uniform nanobelts with 100-200 nm wide and several micrometer long. Their surfaces are very smooth and even. The selected area electron diffraction (SAED) patterns (Figure 3.4b-d) were recorded perpendicular to the growth direction of the three individual nanobelts in Figure 3.4a. They appear as the bright spots of electron diffraction patterns which indicate the single crystalline nanobelts with high crystallinity. All SAED patterns were indexed to correspond with the (001), (101) and (100) planes, comparing to those of the JCPDS standard No. 05-0508 [30]. These suggest that the product is α-MoO_3 nanobelts growing along the [001] direction. The α-MoO_3 nanobelt structure model (insert of Figure 3.4a) grow along the c axis, with the ±(100) top and bottom, ±(010) side, and ±(001) end surfaces [31]. In general, α-MoO_3 composed of distorted MoO_6 octahedrons share both edges along the [001] direction, and corners along the [100] direction. The interaction between layers along the b axis is the weak van der Waals force [28]. In contrast, the interaction along the c axis is strong covalent bond, implying that more energy were released during their growth along the [001] direction. The energy release is in favor with the growth of α-MoO_3 along the c axis. The XRD peaks of the (0k0) planes are higher than those of the corresponding standard, since the (010) plane retained in the final product, as the consequence of slow growing rate [4, 31].

3.1.1.3 FT-IR spectroscopy

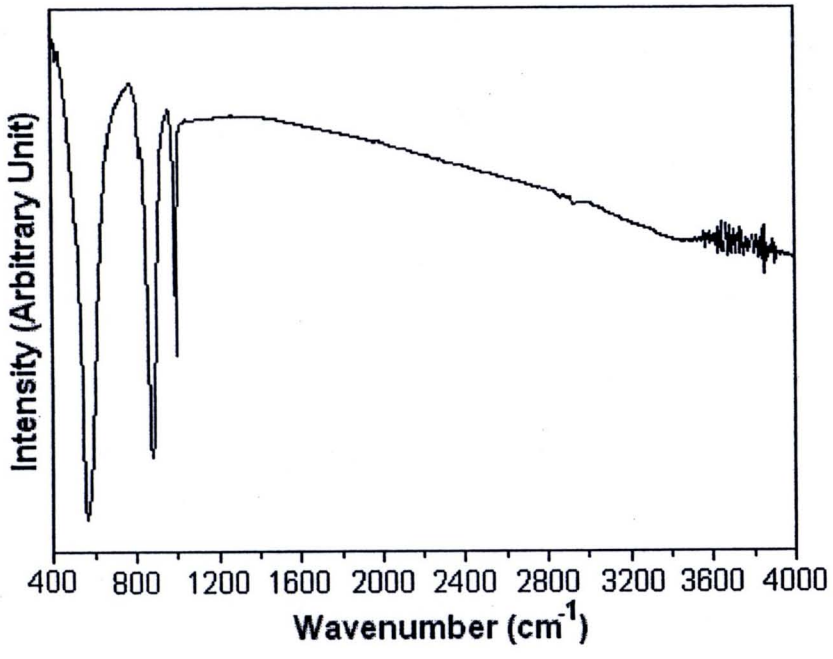

Figure 3.5 FTIR spectra of α-MoO3 nanobelts.

FTIR spectrum (Figure 3.5) of α-MoO_3 nanobelts shows the vibrational interaction between molybdenum and oxygen atoms in α-MoO_3 nanobelts. The sharp band at 996 cm^{-1} is assigned to be the Mo=O stretching vibration, specified as the layered structured α-MoO_3 phase. The vibration band at 882 cm^{-1} corresponds to the stretching vibration of symmetric oxygen atoms arrangement around molybdenum atom in the $[MoO_6]^{6-}$ units. The band at 570 cm^{-1} was caused by the stretching vibration of O atom linked to three metal atoms. The well known O–Mo–O stretching modes were also detected at 813-822 cm^{-1} [26-27, 32-34].

3.1.1.4 Raman spectroscopy

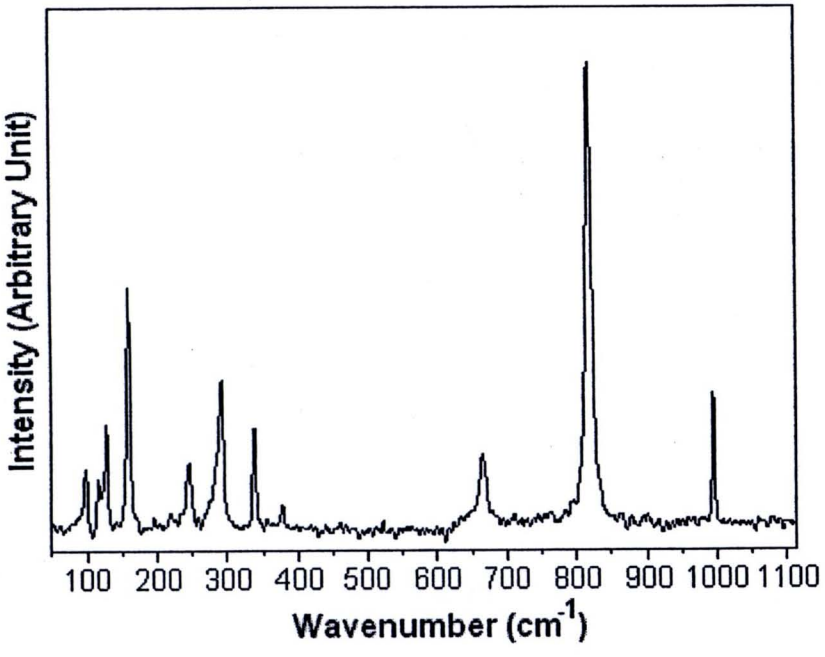

Figure 3.6 Raman spectra of α-MoO_3 nanobelts.

The α-MoO_3 is a layer structure with aba stacking, which contains edge and corner-linked octahedrons. The Mo^{6+} ions occupy in octahedral interstices within the lattice of O^{2-} ions. Layered α-MoO_3 structure is composed of one Mo atom and three nonequivalent types of O atoms, namely, O_1, O_2, and O_3. The Mo–O_1 is the shortest bond with 1.67 Å long. In the c axis, there are two equal Mo–O_2 bonds with 1.95 Å long, and the third bond is in the b axis with 2.33 Å long. Along the a axis, there are two Mo–O_3 bonds with 1.73 and 2.23 Å long [35]. Optical vibrational modes of molybdenum oxide with $D_{2h}{}^{16}(P_{bnm})$ space group is given as follows.

$$\Gamma = 8A_g + 8B_{1g} + 4B_{2g} + 4B_{3g} + 4A_u + 3B_{1u} + 7B_{2u} + 7B_{3u} \qquad (1)$$

where A_g, B_{1g}, B_{2g}, and B_{3g} are Raman-active modes, A_u is an inactive mode, and B_{1u}, B_{2u} and B_{3u} are infrared-active modes [35-36]. The Raman spectrum of α-MoO_3 operated using 632.8 nm wavelength of He-Ne laser at 50-1100 cm^{-1} wavenumber is shown in Figure 3.6. The Raman spectrum of α-MoO_3 was classified into stretching, deformation, and lattice modes at 600-1000, 200–400, and below 200 cm^{-1}, respectively. Below 200 cm^{-1}, the peak at 159 cm^{-1} is the A_g mode, corresponding to the $\delta(O_2Mo_2)_n$ polyhedrons along with the chain axis. Its intensity was strongly increased by the polarization along the c axis. The peaks at 98, 116, and 127 cm^{-1} were assigned to be the B_{1g}, B_{2g}, and B_{3g} modes, respectively. At 200-400 cm^{-1} wavenumber, the 245, 292, 338 and 379 cm^{-1} peaks were detected. The peak at 292 cm^{-1} is the B_{3g} mode corresponding to the $\delta O_1=M=O_1$ wagging. Those at 338 and 379 cm^{-1} are the A_g and B_{1g} modes which correspond to the $\delta O_2–M–O_2$ scissor. The peak at 471 cm^{-1} is the A_g mode which corresponds to the ν_{as} $M–O_2$ stretching and bending. The Raman peaks at 816 and 992 cm^{-1} are the A_g modes. These are assigned to be the ν_s $Mo–O_3–Mo$ stretching of which the bonding aligns along the a axis, and ν_{as} $Mo = O_1$ stretching of which the bonding aligns along the b axis [35-38]. Different Raman vibration modes of α-MoO_3 nanobelts of the present research in comparison with those of other reports are shown in Table 3.2.

Table 3.2 Raman vibration modes of α-MoO_3 nanobelts.

Raman vibration	Assignment	Wavenumber (cm^{-1})					
		Our work	Ref. 39	Ref. 40	Ref. 41	Ref. 28	Ref. 42
A_g	Transnational rigid MoO_4	83	84	84	82	82	83
B_{2g}	Transnational rigid MoO_4	98	100	98	-	98	99
B_{2g}	Translational rigid MoO_4	116	117	117	115	114	116
B_{3g}	Translational rigid MoO_4	128	129	129	129	128	129
A_g/B_{1g}	$\delta(O_2Mo_2)_n$	159	159	158	158	156	156
B_{2g}	δO_2-Mo-O_2 scissor	196	197	197	198	197	198
A_g	δO_2-Mo-O_2 scissor	218	217	218	216	216	217
B_{3g}	δO_1-Mo-O_1 wagging	245	246	244	246	244	246
B_{2g}	δO_1-Mo-O_1 wagging	283	283	283	284	282	283
B_{3g}	δO_2-Mo-O_2 scissor	292	291	291	-	-	291
B_{1g}	δO_3-Mo-O_3 deformation	338	338	337	336	336	337
A_{1g}	δO_2-Mo-O_2 scissor	365	366	365	365	364	365
B_{1g}	δO_2-Mo-O_2 scissor	379	378	378	378	376	379
A_g	δ_{as}Mo-O_2-Mo bending	-	417	473	-	469	473
B_{2g}	ν_{as}Mo-O_2-Mo stretching	664	666	666	666	666	666
A_g	ν_sMo-O_3-Mo stretching	818	819	819	819	818	819
A_g	ν_{as}Mo=O_1 stretching	995	995	996	996	993	995

3.1.1.5 The formation of α-MoO_3 nanobelts

The formation mechanism of α-MoO_3 nanobelts form isopolymolybdate $(Mo_7O_{24})^{6-}$ anions under hydrothermal treatment was reported by X.W. Lou and H.C. Zeng [43] as shown in equation (2)

$$Mo_7O_{24}^{6-} + 6H^+ \rightarrow 7MoO_3 + 3H_2O \quad (2)$$

The $Mo_7O_{24}^{6-}$ anions were obtained by dissolving of $(NH_4)6Mo_7O_{24}\cdot 4H_2O$ as starting material in acidic solution. The overall equilibrium would shift the hydrothermal reaction to the right, although many intermediate steps (and thus compounds/phases) may exist. However, T. Xia et al. [44] suggested the growth of 1D α-MoO_3 nanostructures by electroneutral and dehydration reactions, which are formulated as follows.

$$Mo_7O_{24}^{6-} + 6H^+ + 11\ H_2O \rightarrow 7MoO_3\cdot 2H_2O \quad (3)$$

By increasing the temperature, water was released from 229 $MoO_3\cdot 2H_2O$ by the flowing reactions.

$$MoO_3\cdot 2H_2O \rightarrow \alpha\text{-}MoO_3\cdot H_2O + H_2O \quad (4)$$

$$MoO_3\cdot H_2O \rightarrow \alpha\text{-}MoO_3 + H_2O \quad (5)$$

The crystal structure of $MoO_3\cdot 2H_2O$ is monoclinic symmetry and does not display any one-dimensional chain structure. α-$MoO_3\cdot H_2O$ exhibits Mo-O-Mo chains running along the [001] direction. For α-MoO_3, it has the maximum intensity of one-dimensional growth due to the presence of two different sorts of chains along the a and c axes, respectively.

3.1.1.6 Optical property of α-MoO_3 nanobelts

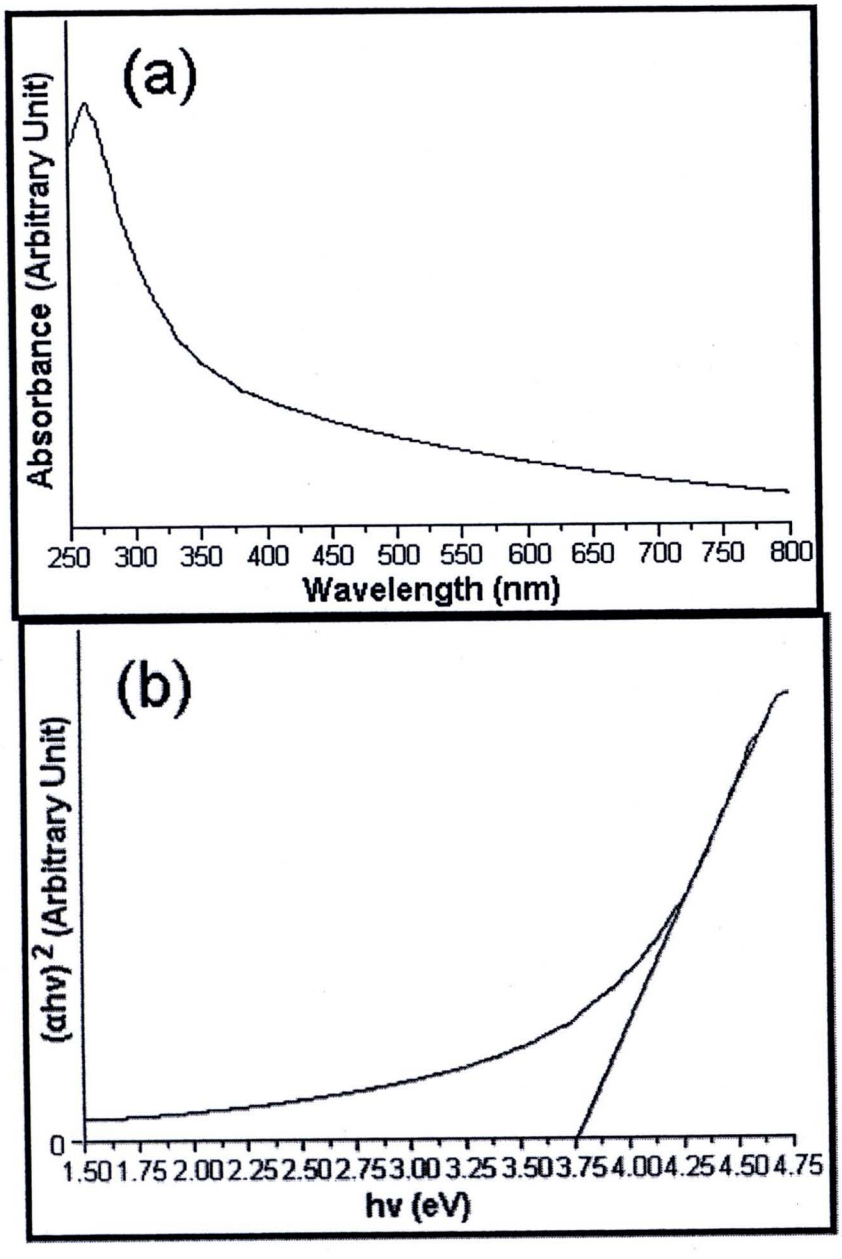

Figure 3.7 (a) UV absorbance, and (b) the $(\alpha h\nu)^2$ versus hν plot of α-MoO_3 nanobelts.

The optical absorption spectrum of α-MoO_3 nanobelts (Figure 3.7a) exhibits the strong absorption centered at ~262 nm in the UV region, due to the charge transfer in the $[MoO_6]^{6-}$ octahedrons [45]. The direct band gap (E_g) was calculated from the relation between the absorption coefficient and photon energy given by

$$h\nu\alpha = (h\nu - E_g)^n \quad (8)$$

where α, h, ν, and E_g are the absorbance, Planck constant, photon frequency, and optical band gap, respectively. The parameter n is a constant associated with the different types of electronic transitions: n = 1/2, 2, 3/2 or 3 for direct allowed, indirect allowed, direct forbidden and indirect forbidden transitions, respectively [46]. Figure 3.7b shows the plot of $(\alpha h\nu)^2$ versus hν. The direct Eg of α-MoO_3 nanobelts was determined to be 3.75 eV, larger than that of the bulk state of 2.9 eV [47]. Generally, the origin of these energy states of materials is caused by the formation of oxygen vacancies in the structure, and consequently the symmetry between the (lattice former)–O bonds breaks down. The increase in band gap can be attributed by the reduction of oxygen deficiency 343 and the α-MoO_3 nanobelts approach the stoichiometric state [45-46].

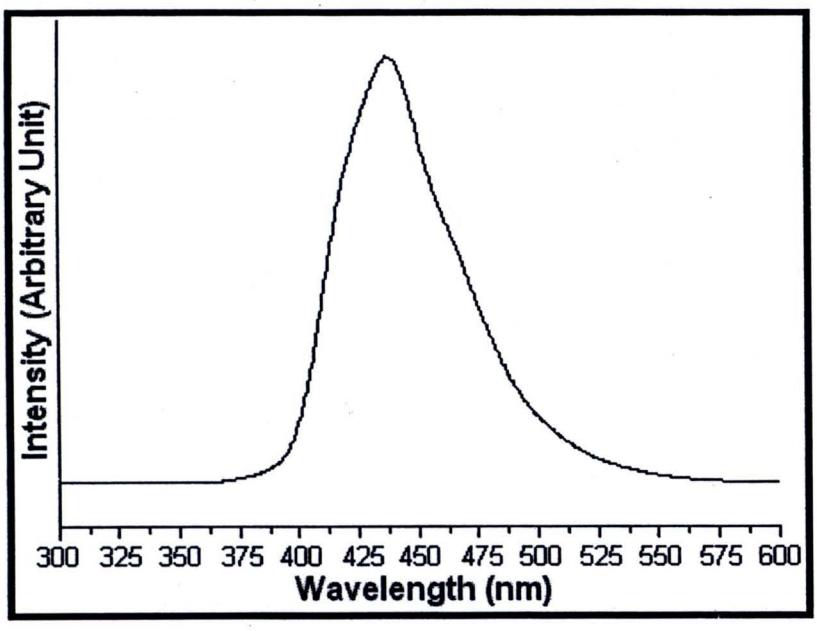

Figure 3.8 PL emission of α-MoO_3 nanobelts at room temperature

Figure 3.8 is a photoluminescence spectrum of α-MoO_3 nanobelts excited by the 337 nm wavelength at room temperature. It shows a broad peak at 375-550 nm, corresponding to the report of Song et al. [48], with the maximum emission peak at 437 nm due to the $O_{2p} \rightarrow Mo_{4d}$ charge transition of α-MoO_3 nanobelts [49].

3.1.2 The effect of reaction temperature, holding time and type of acid on the formation of α-MoO_3 nanobelts.

3.1.2.1 The effect of reaction temperature

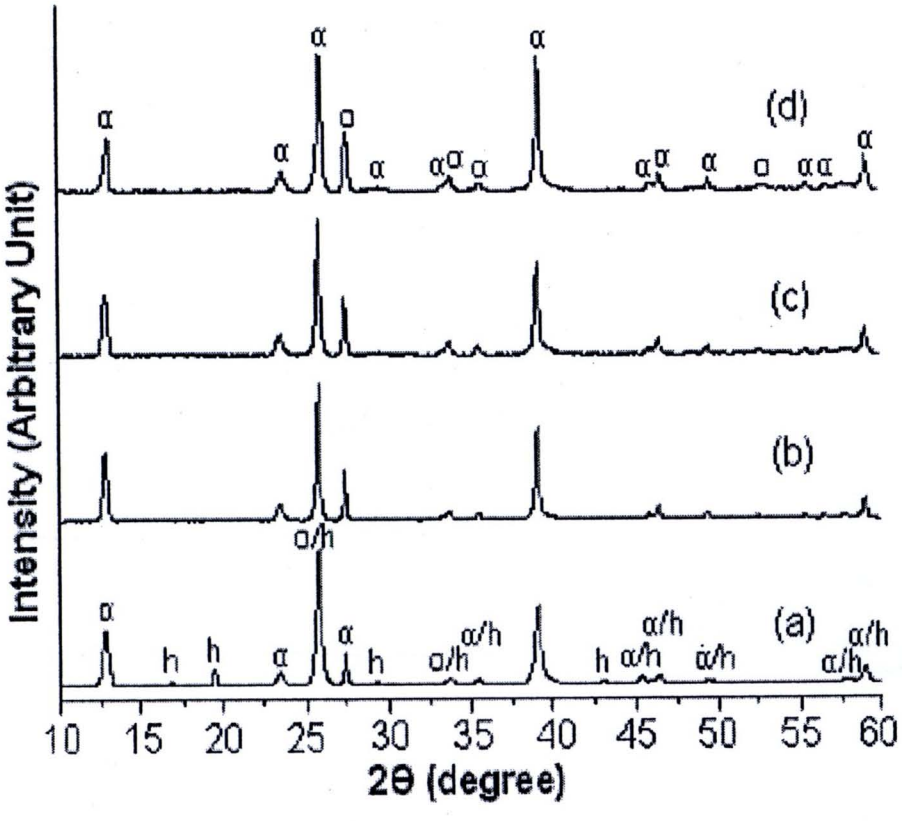

Figure 3.9 XRD patterns of α-MoO_3 nanostructures under hydrothermal at (a) 120, (b) 140, (c) 160 and (d) 160 °C, respectively for 20 h.

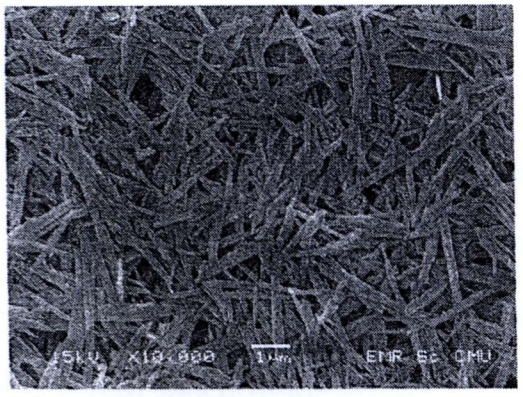

(a)

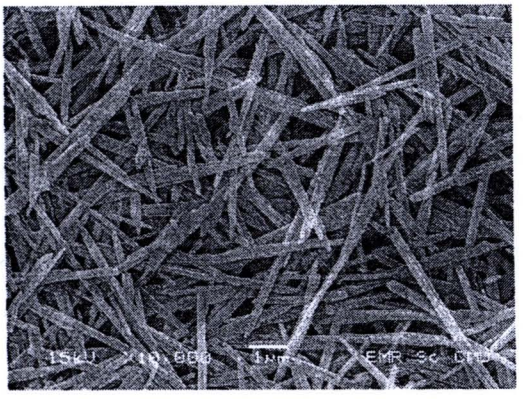

(b)

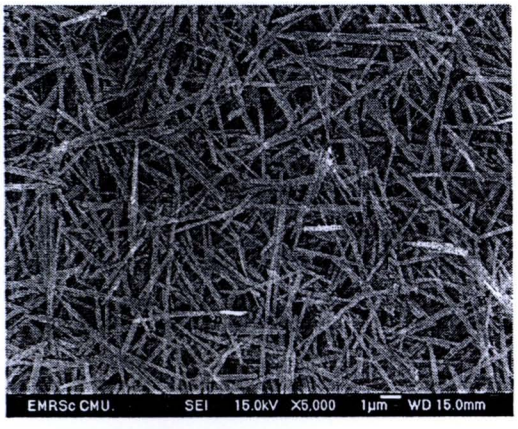

(c)

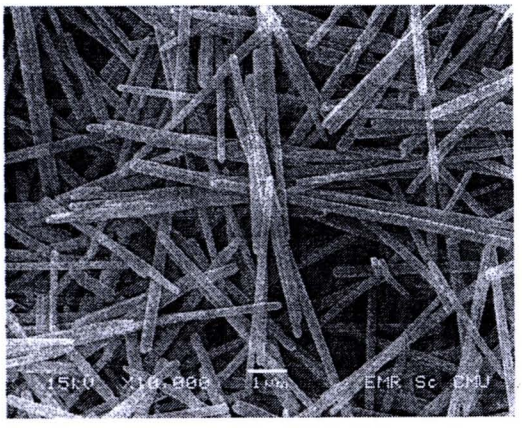

(d)

Figure 3.10 SEM images of α-MoO_3 nanostructures under hydrothermal at (a) 120, (b) 140, (c) 160 and (d) 180 °C, respectively for 20 h.

The effect of reaction temperature, holding time and type of acid were studied during the formation of α-MoO_3 nanobelts. Figure 3.9 and 3.10 show the XRD patterns and SEM images of α-MoO_3 nanobelts, which were synthesized by hydrothermal method at 100-180 °C for 20 h. XRD analysis proved that the product at 100 °C for 20 h is composed of mixed phase of hexagonal MoO_3 (h-MoO_3) and α-MoO_3 corresponding to the JCPDS No. 21-0569 [30] for h-MoO_3, and 05-0508 [30] for α-MoO_3, with no detection of any other impurities. The h-MoO_3 phase became lessen when the reaction hydrothermal temperature was increased. The pure α-MoO_3 phase was produced at 140 °C and above. The α-MoO_3 nanobelts were agglomerated as nanobelt bundles at 100-160 °C for 20 h, and separated into individual uniform nanobelts at 180 °C for 20 h.

3.1.2.2 The effect of holding time

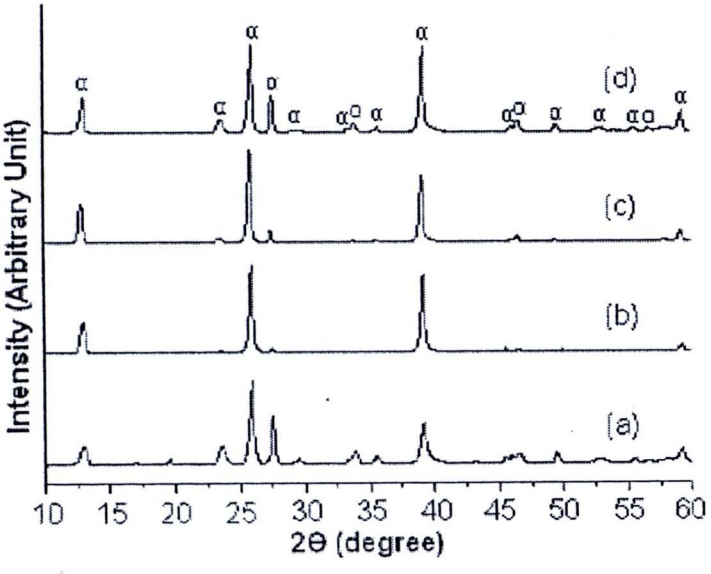

Figure 3.11 XRD patterns of α-MoO_3 nanostructures under hydrothermal at 180 °C for (a) 2, (b) 5 (c) 10 and (d) 20 h, respectively.

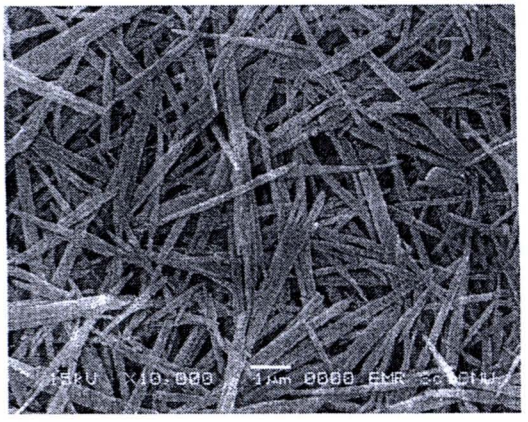

(a)

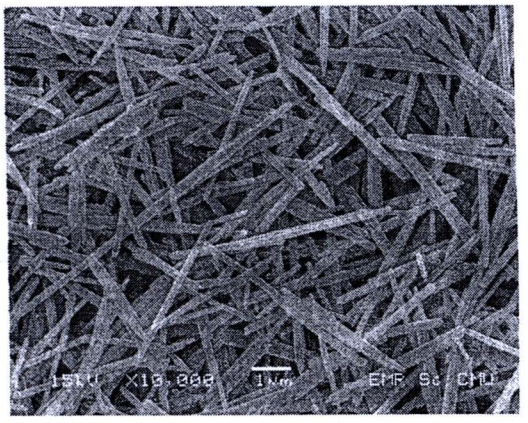

(b)

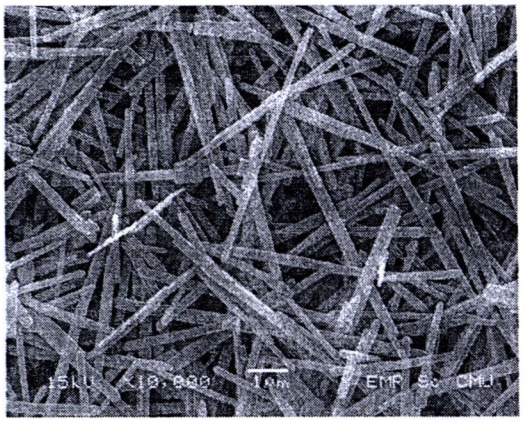

(c)

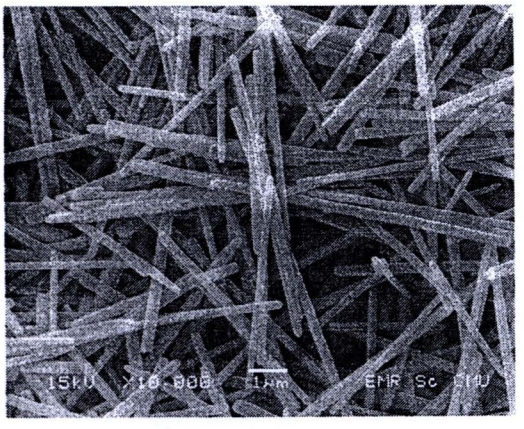

(d)

Figure 3.12 SEM images of α-MoO_3 nanostructures under hydrothermal at 180 ^{o}C for (a) 2, (b) 5 (c) 10 and (d) 20 h, respectively

Figure 3.11 and 3.12 show the XRD patterns and SEM images of α-MoO_3 nanobelts synthesized by hydrothermal method at a constant temperature (180 °C) for 2-20 h. When the reaction time was decreased to 5 h, the product remained as pure α-MoO_3 phase. The mixtures of h-MoO_3 and α-MoO_3 as minor and major phases were detected, when the length of time was reduced to be 2 h. At this stage (180 °C, 2 h), the agglomerated bundle of nanobelts was produced. For longer time (5-10 h), the α- MoO_3 nanobelts were separated, but composed of the mixture of nano- and micro-belts. Consequently, the uniform α-MoO_3 nanobelts were produced at 180 °C for 20 h.

3.1.2.3 The effect of types of acid

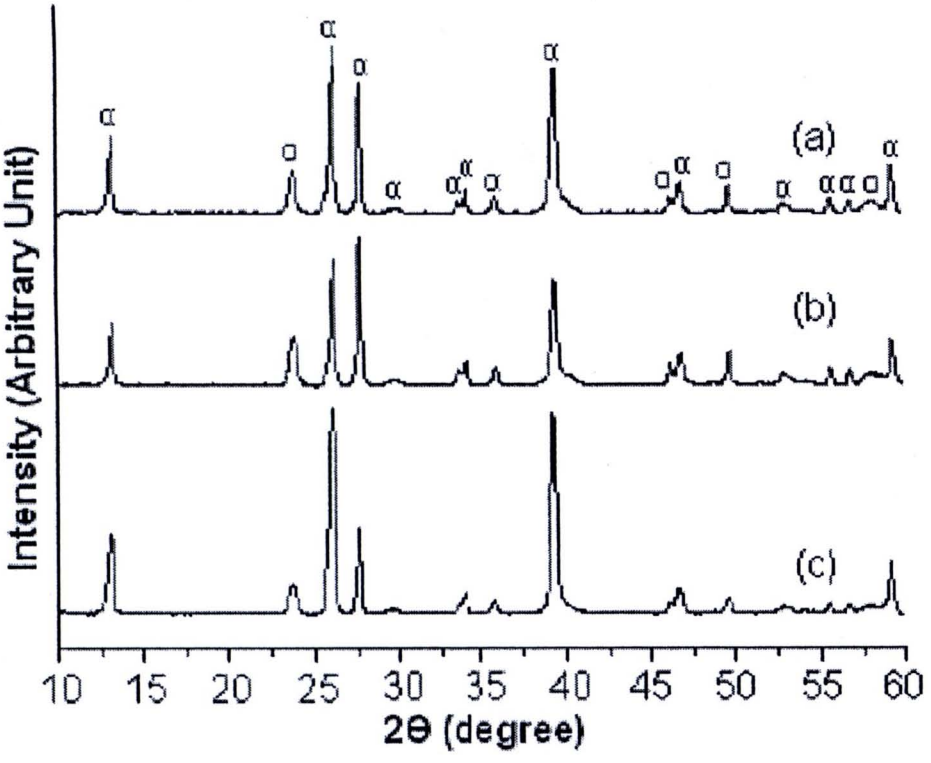

Figure 3.13 XRD patterns of α-MoO_3 nanostructures under hydrothermal at 180 °C for 20 h using (a) HNO_3, (b) HCl and (c) H_2SO_4, respectively.

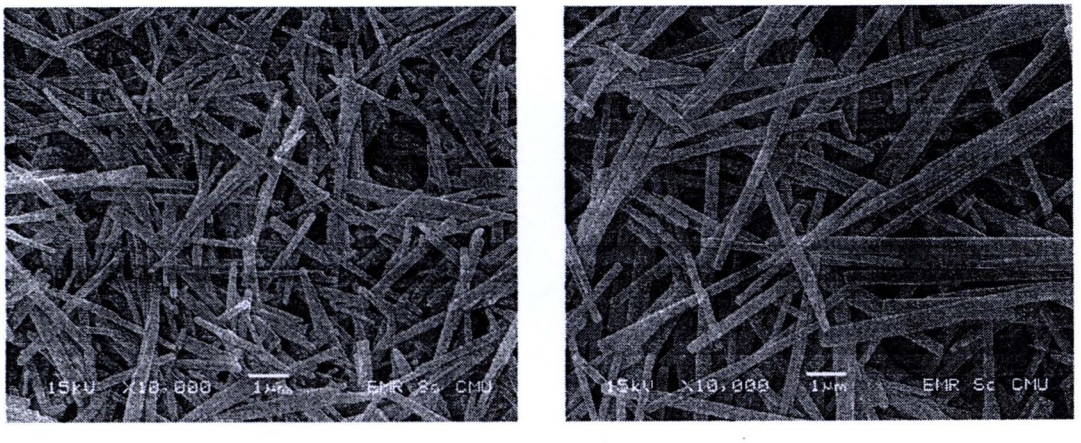

(a) (b)

Figure 3.14 SEM images of α-MoO_3 nanostructures under hydrothermal at 180 °C for 20 h using (a) HCl and (b) H_2SO_4.

When either HCl or H_2SO_4 instead of HNO_3 was used, the XRD patterns (Figure 3.13) remained the same, excluding intensities of the diffraction peaks. The XRD patterns also corresponded to the pure phase of α-MoO_3, but all intensities of the diffraction peaks of α-MoO_3 for using of HCl and H_2SO_4 became lessened – lowering the degree of crystallinity. The products produced in the HCl and H_2SO_4 acidic solutions, shown by SEM images (Figure 3.14), are short agglomerated α-MoO_3 nanobelts.

These proved that the reaction hydrothermal temperature, holding reaction time and types of acid are the key factors used to control pure phase and uniform α-MoO_3 nanobelts. In general, the nanomaterials with high crystallinity and uniform morphology have the potential to improve the photoluminescent properties. Therefore, the best condition for the synthesis of uniform α-MoO_3 nanobelts with high crystallinity in this research is the 180 ^{o}C and 20 h hydrothermal heating of the solution containing 15 ml 2 M HNO_3.

3.2 Silver composited on Molybdenum Oxide nanobelts synthesized by a Sonochemical method

3.2.1 X-ray diffraction

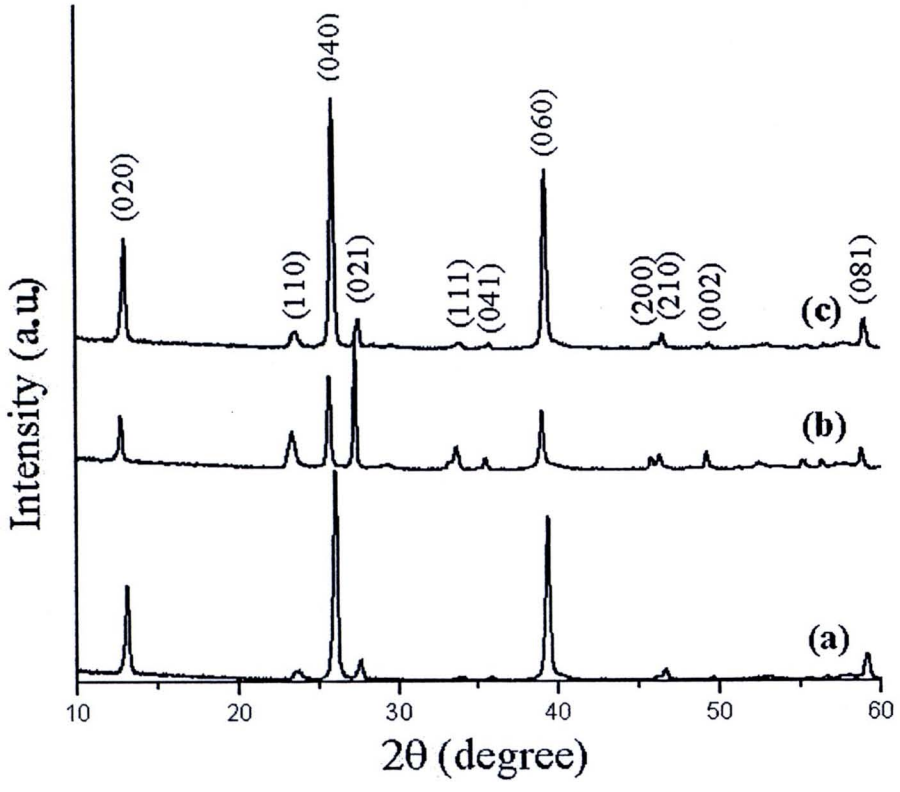

Figure 3.15 XRD patterns of α-MoO_3/Ag composites under ultrasonic irradiation maintained at room temperature for 20 min with the coatings of (a) 1 wt%, (b) 5 wt% and (c) 10 wt% of Ag.

Figure 3.15 shows the XRD patterns of α-MoO_3/Ag composites under ultrasonic irradiation maintained at room temperature for 20 min with the coatings of 1-10 wt% of silver. All the diffraction peaks can be indexed to pure α-MoO_3 phase which was exactly agree with those of the JCPDS No. 05-0508 [30]. No peaks of any other phases were detected which indicated the purity of the final product.

3.2.2 Scanning and transmition electron microscopy

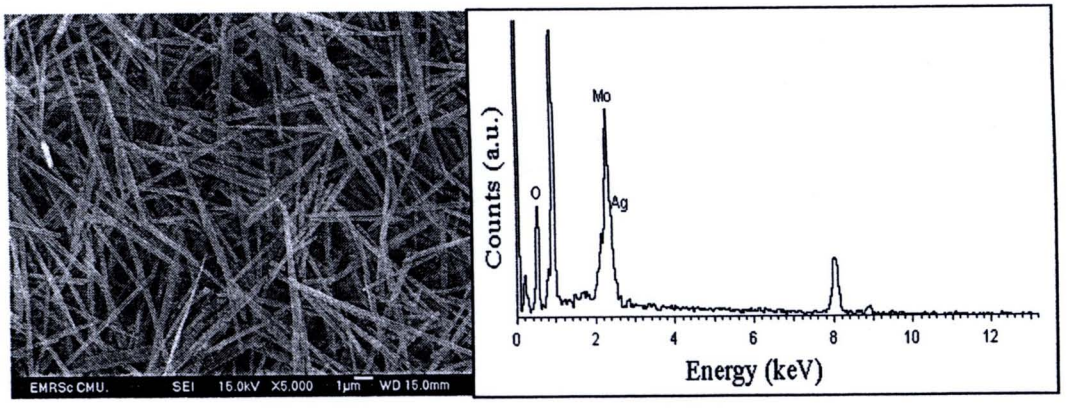

(a)

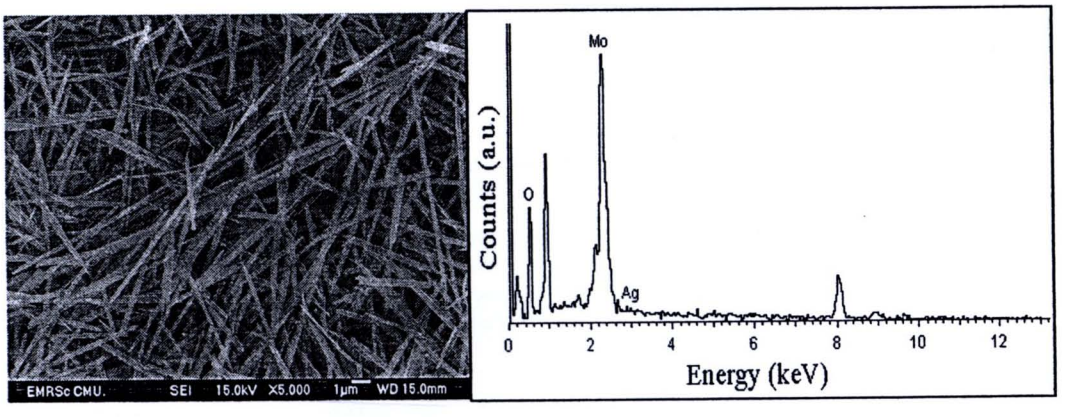

(b)

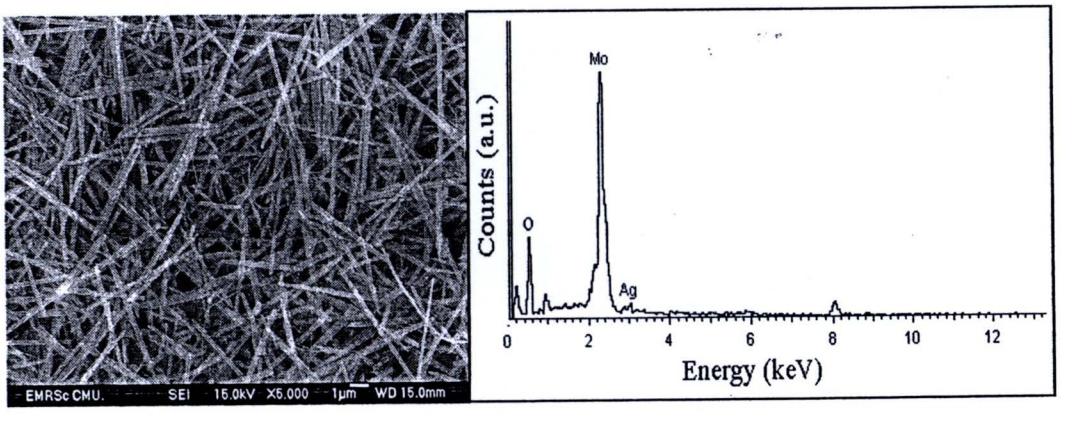

(c)

Figure 3.16 SEM images and EDS spectra of α-MoO_3/Ag composite under ultrasonic irradiation maintained at room temperature for 20 min with the coatings of (a) 1 wt%, (b) 5 wt% and (c) 10 wt% of Ag.

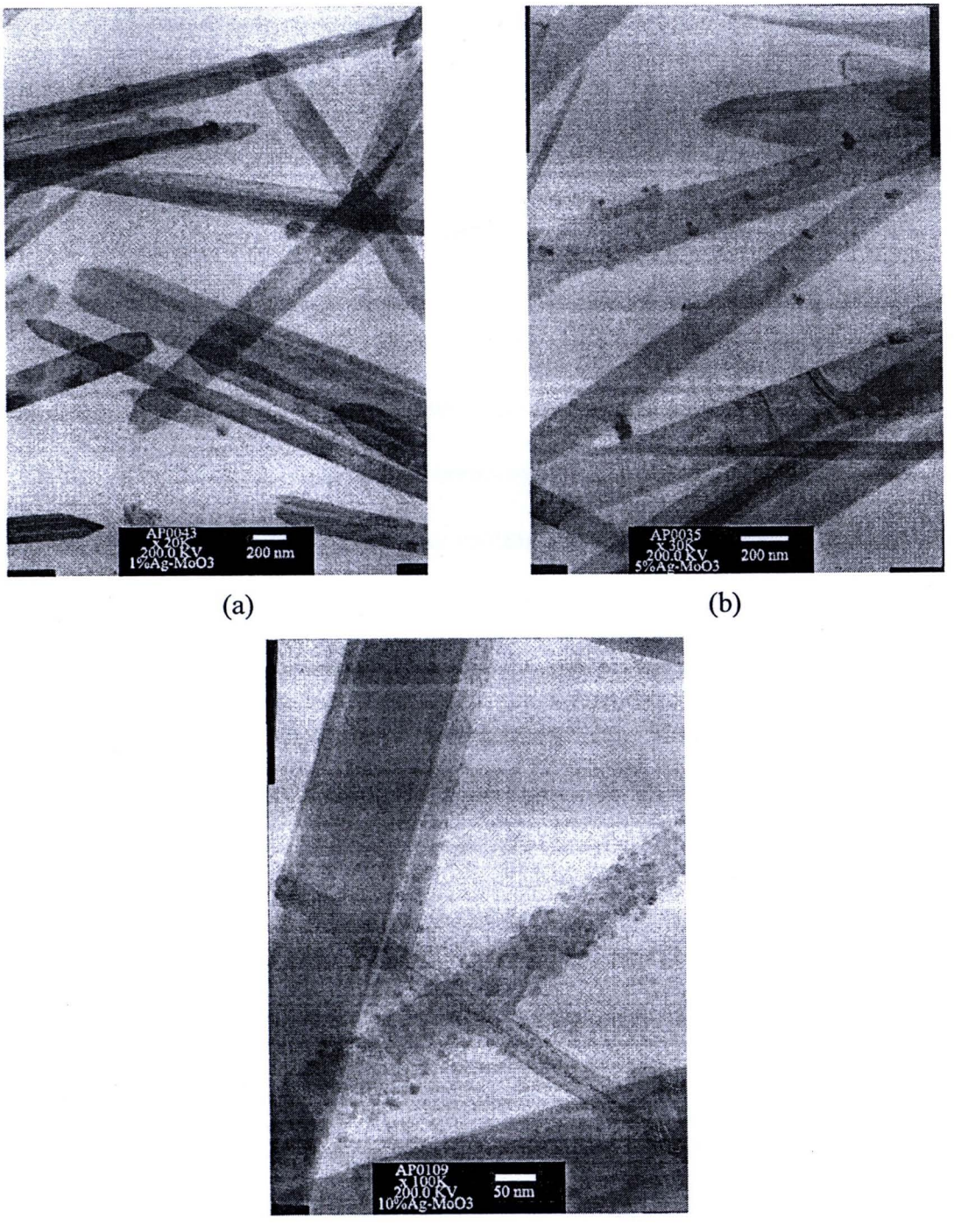

(a) (b)

(c)

Figure 3.17 TEM images of α-MoO_3/Ag composites under ultrasonic irradiation maintained at room temperature for 20 min with the coatings of (a) 1 wt%, (b) 5 wt% and (c) 10 wt% of Ag.

Figure 3.16 shows the SEM images and EDX spectra of α-MoO_3/Ag composites under ultrasonic irradiation maintained at room temperature for 20 min. SEM image shows α-MoO_3 nanobelts without the detection of Ag nanoparticles deposited on nanobelts because these nanoparticles are very tiny(nanoscale). The EDS spectrum show the Mo, O (with atomic ratio of 1:3), and Ag were detected. Percent atomic of silver are 0.19, 0.29, and 1.00% for the coatings containing (a) 1 wt%, (b) 5 wt% and (c) 10 wt% of silver respectively. Detailed morphology of α-MoO_3/Ag composited structure was proved by TEM images (Figure 3.17), which show Ag coatings on α-MoO_3 nanobelts, for the coatings of 1-5 wt% Ag coating on α-MoO_3 nanobelts. The number of Ag nanoparticles were increased with the increasing in the wt% of silver coating on the nanobelts. At 10 wt% Ag, the nanoparticles number are as the highest, and their average sizes are ~10 nm.

3.2.3 Raman spectroscopy

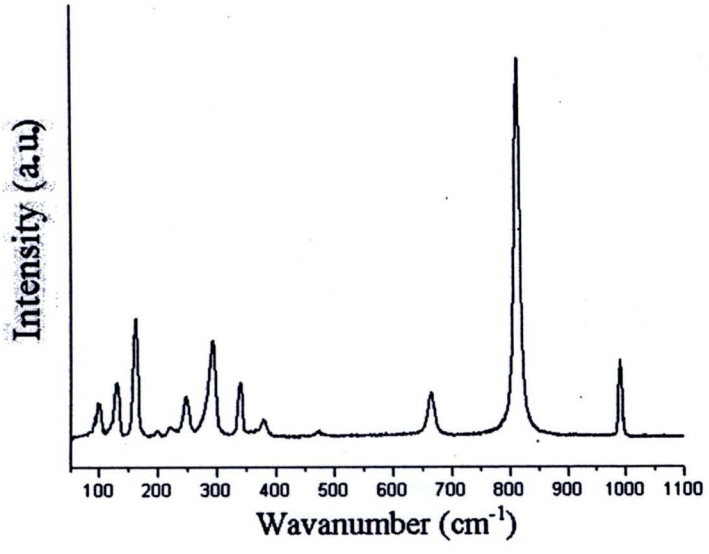

Figure 3.18 Raman spectrum of α-MoO_3/Ag composites for the coatings of 10 wt% of silver.

The Raman spectrum of α-MoO_3/Ag composites over the range of 50-1100 cm^{-1} is shown in figure 3.18. The Raman spectrum of α-MoO_3 was classified into stretching, deformation, and lattice modes at 600-1000, 200–400, and below 200 cm^{-1}, respectively. The peak at 159 cm^{-1} is the $\delta(O_2Mo_2)_n$ polyhedrons along with the chain axis. Its intensity was strongly increased by the polarization along the c axis. The peak at 292 cm^{-1} is the $\delta O_1{=}M{=}O_1$ wagging. Those at 338 and 379 cm^{-1} are the $\delta O_2{-}M{-}O_2$ scissor. The peak at 471 cm^{-1} is the ν_{as} $M{-}O_2$ stretching and bending. The Raman peaks at 816 and 992 cm^{-1} are the ν_s $Mo{-}O_3{-}Mo$ stretching of which the bonding aligns along the a axis, and ν_{as} $Mo = O_1$ stretching with the bonding aligns along the b axis [35-38].

3.2.4 Optical property

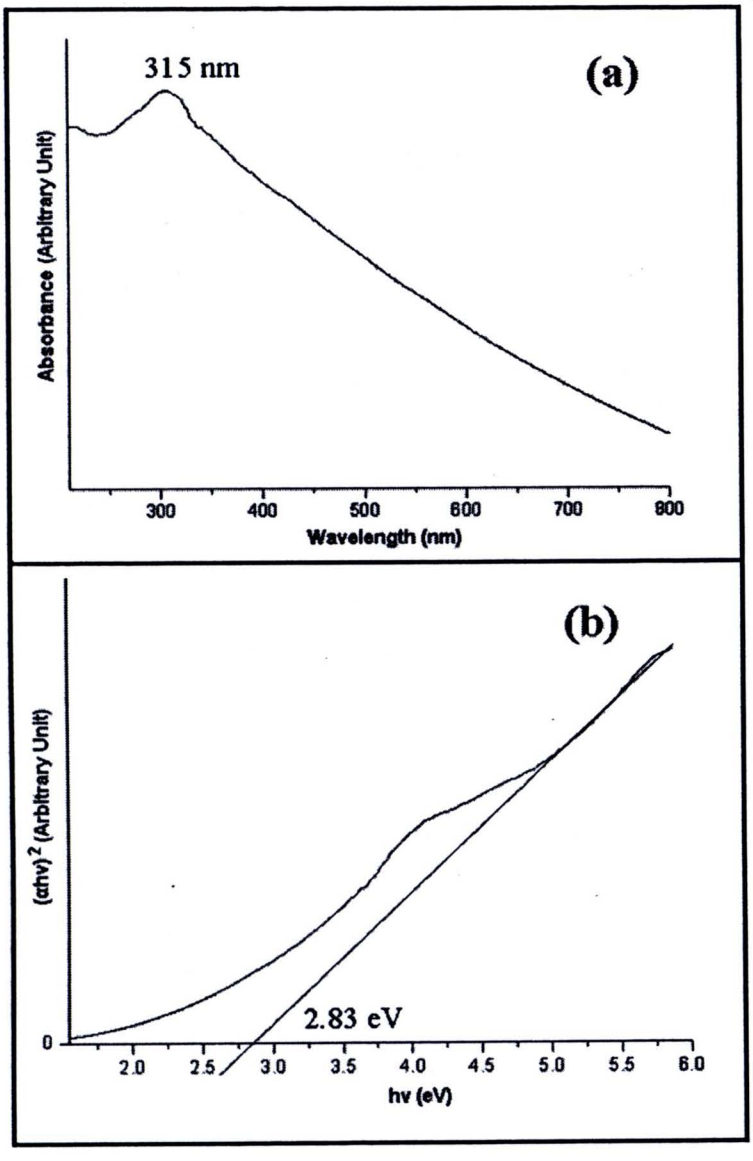

Figure 3.19 (a) UV absorbance, and (b) the $(\alpha h\nu)^2$ versus hν plot of α-MoO_3/Ag composites for the coatings of 10 wt% of Ag.

UV–vis absorbance α-MoO_3/Ag composites (Figure 3.19a) show an absorption band in the 200–800nm range. No absorption band in the visible range was detected. Its direct energy gap was determined by extrapolation of the linear portion of the curve (Figure 3.19b) to $\alpha = 0$, corresponding to 2.83 eV.